



HAL
open science

Validation Of Anatomical Models To Study Aerosol Deposition In Human Nasal Cavities

Sandrine Le Guellec, Deborah Le Penneec, Stéphane Gatier, Lara Leclerc, Maria Cabrera, Jérémie Pourchez, Patrice Diot, Grégory Reyckler, Laurent Pitance, Marc Durand, et al.

► **To cite this version:**

Sandrine Le Guellec, Deborah Le Penneec, Stéphane Gatier, Lara Leclerc, Maria Cabrera, et al.. Validation Of Anatomical Models To Study Aerosol Deposition In Human Nasal Cavities. *Pharmaceutical Research*, 2014, 31 (1), pp.228-237. 10.1007/s11095-013-1157-6 . hal-01139263

HAL Id: hal-01139263

<https://hal.science/hal-01139263v1>

Submitted on 27 Nov 2024

HAL is a multi-disciplinary open access archive for the deposit and dissemination of scientific research documents, whether they are published or not. The documents may come from teaching and research institutions in France or abroad, or from public or private research centers.

L'archive ouverte pluridisciplinaire **HAL**, est destinée au dépôt et à la diffusion de documents scientifiques de niveau recherche, publiés ou non, émanant des établissements d'enseignement et de recherche français ou étrangers, des laboratoires publics ou privés.

Validation of Anatomical Models to Study Aerosol Deposition in Human Nasal Cavities

Sandrine Le Guellec · Deborah Le Pennec · Stephane Gatier · Lara Leclerc · Maria Cabrera · Jeremie Pourchez · Patrice Diot · Gregory Reychler · Laurent Pitance · Marc Durand · François Jamar · Laurent Vecellio

Received: 26 March 2013 / Accepted: 22 July 2013 / Published online: 25 September 2013
© The Author(s) 2013. This article is published with open access at Springerlink.com

ABSTRACT

Purpose Intranasal deposition of aerosols is often studied using *in vitro* nasal cavity models. However, the relevance of these models to predict *in vivo* human deposition has not been validated. This study compared *in vivo* nasal aerosol deposition and *in vitro* deposition in a human plastinated head model (NC1) and its replica constructed from CT-scan (NC2).

Methods Two nebulizers (Atomisor Sonique® and Easynose®) were used to administer a 5.6 μm aerosol of ^{99m}Tc-DTPA to seven healthy volunteers and to the nasal models. Aerosol deposition was quantified by γ-scintigraphy in the nasal, upper nasal cavity and maxillary sinus (MS) regions. The distribution of aerosol deposition was determined along three nasal cavity axes (x, y and z).

Results There was no significant difference regarding aerosol deposition between the volunteers and NC1. Aerosol deposition was significantly lower in NC2 than in volunteers regarding nasal region ($p < 0.05$) but was similar for the upper nasal cavity and MS regions. Mean aerosol distribution for NC1 came within the standard deviation (SD) of *in vivo* distribution, whereas that of NC2 was outside the *in vivo* SD for x and y axes.

Conclusions In conclusion, nasal models can be used to predict aerosol deposition produced by nebulizers, but their performance depends on their design.

KEY WORDS aerosol · anatomical model · nasal · nebulizer

INTRODUCTION

The development of therapies for intranasal delivery involves three major fields of interest linked to pharmaceutical targeting: topical, systemic and more recently central nervous system action.

Topical administration is used to treat nasal congestion (or obstruction) and inflammation of the nasal mucosa during acute or chronic pathologies such as allergic rhinitis, rhinosinusitis and nasal polyposis. High doses of medication can be delivered whereas adverse effects are minimized (1). Topical nasal delivery is also safer than traditional administration routes or even lung

S. Le Guellec · L. Vecellio (✉)
DTF-Aerodrug, Faculté de Médecine Bâtiment M, 10 ter bd Tonnellé
F-37032 Tours, France
e-mail: vecellio@med.univ-tours.fr

S. Le Guellec · D. Le Pennec · M. Cabrera · P. Diot · L. Vecellio
EA6305, CEPR, Faculté de Médecine, Université François Rabelais
F-37032 Tours, France

S. Gatier
DTF-Medical F-42003 Saint Etienne, France

L. Leclerc · J. Pourchez
Ecole Nationale Supérieure des Mines CIS-EMSE, LINA EA 4624
F-42023 Saint-Etienne, France

L. Leclerc · J. Pourchez · M. Durand
Université Jean Monnet, Faculté de Médecine LINA EA 4624
SFR IFRESIS F-42023 Saint-Etienne, France

P. Diot
Service de Pneumologie, CHRU de Tours F-37044 Tours, France

G. Reychler · L. Pitance
Service de Pneumologie, Cliniques Universitaires Saint-Luc, UCL
1200 Brussels, Belgium

M. Durand
Service d'ORL et de Chirurgie Cervico-Faciale, Centre Hospitalier
Emile-Roux F-43012 Le Puy-en-Velay, France

F. Jamar
Service de Médecine Nucléaire, Cliniques Universitaires Saint-Luc, UCL
1200 Brussels, Belgium

inhalations for vaccines (2,3). The large surface area of nasal mucosa is also an advantage for intranasal systemic delivery, in particular for peptides (vitamins), macromolecules, opioids and also antimigraine drugs (4,5).

Potential use of the nasal route to deliver medications to the brain has been widely investigated, in particular for morphine and also several peptides and proteins (6–8) or Tacrine®, a cholinesterase inhibitor currently being developed to treat Alzheimer's disease, which has a very low oral bioavailability (9,10).

The efficacy of a given nasal treatment will depend on its deposition in the nose, because the pharmaceutical target (local, systemic, brain) is directly related to a specific nasal anatomical site. For example, the middle meatus, the maxillary sinuses and the ethmoid regions have been identified as important drug delivery target sites for local treatment of inflammation and infection in rhinological pathologies (11). Systemic delivery is enhanced by exposing the drug to the respiratory zone of the nasal cavities, *i.e.* the middle and inferior turbinates, the septum and nasal floor around the turbinates, rather than the olfactory epithelium (5). The respiratory zone has a large surface area (120 to 150 cm²) and is highly vascularized *via* the posterior lateral branches of the sphenopalatine artery and large venous sinusoids (5,12). The anatomic connections between the nose and the brain compartments lie in passages either *via* the route [olfactory bulb (within the ethmoid (nose)/trigeminal neural pathways (brain)] or through the brain blood barrier *via* the peripheral circulation (systemic passage) (13,14).

In order to develop drug formulations for intranasal delivery, both device and particle-related factors that optimize delivery to the target sites must be determined (11).

Particles larger than 10 µm inhaled nasally are known to deposit in the nasal cavities (15) but there are no guidelines or international consensus regarding the relationship between aerosol characteristics and the precise deposition site within the nasal cavities.

The delivery system and the administration technique also play a role in the nasal deposition. For example, we demonstrated in a previous study that two aerosols with the same particle size produced by two different nebulizers, *e.g.* mesh *vs.* jet, may strongly differ in terms of nasal deposition (16).

Therefore, *in vitro* metrology methods based on particle size measurements do not allow one to predict with precision the deposition of nasally inhaled drugs.

Intranasal deposition can be measured *in vivo* by gamma camera imaging. However, such studies are restricted by the risk of exposure to radiation and ethical considerations. As an alternative, anatomical models such as cadaver heads (17,18), nasal cavity replicas (19,20) or nasal casts using recent prototyping techniques (fused deposition modelling (FDM) or stereolithography (*e.g.* the SLA, Viper or SAINT models) (21,22) have been developed. However, to our knowledge,

these models have never been validated to predict *in vivo* human aerosol deposition.

The aim of this study was to assess by gamma camera techniques the value of anatomical models to predict *in vitro* aerosol deposition in the nose, comparing the data to those obtained *in vivo* in healthy volunteers. Two kinds of nasal model were tested, a plastinated head (cadaver head) and a nasal cast based on fused deposition modelling technology. Two types of aerosol generator were used, a jet and a mesh nebulizer.

MATERIALS AND METHODS

Nebulizers

Two nasal nebulizer systems (schematized in Fig. 1) were used: a sonic nasal jet nebulizer (NLI ISN Atomisor sonore®, DTF medical, Saint Etienne, France), and a new nasal mesh nebulizer (Easynose®, DTF medical, Saint Etienne, France) previously described by Vecellio *et al.* (16). The NLI ISN was used with an AOLH® box Atomisor compressor (DTF medical, Saint Etienne, France) generating an additional sound at a frequency of 100Hz. The sonic aerosol was administered in both nostrils simultaneously through a nasal plug and inhaled during the inspiratory phase. The Easynose consists of an Aeroneb® Solo mesh (Aerogen, Galway, Ireland) connected to a specific compressor (DTF medical, Saint Etienne, France); the aerosol was administered through a nasal plug while the patient breathed through the mouth. The volume median diameter of both nebulizers was 5.6 µm, evaluated using a laser diffraction method (Spraytec, Malvern, UK).

The same devices were used for both *in vivo* and *in vitro* studies. For each experiment, nebulizers were loaded with 74 MBq/3 mL of ^{99m}Tc-DTPA (Technescan DTPA, Diethyl-Triamine-Penta-Acetic acid, Mallinckrodt Medical, Petten, Netherlands). The duration of nebulisation was limited to 10 min.

In Vivo Study

Participants were seven healthy, non-smoking male volunteers aged 21 to 36 years, with a mean weight of 77 ± 10 kg and a mean height of 1.81 ± 0.03 m. This study forms part of a large research programme, and a series of data involving the same participants has already been published (16), but the data reported hereafter had not reported in this previous paper. The present study was carried out in a single centre (ENT department of the hospital of Louvain, Brussels, Belgium). The study protocol was approved by the Ethics Committee of the hospital and the Medical School of Louvain University, and by the regulatory authorities. In accordance with the Declaration of Helsinki and with the current guidelines for Clinical Good

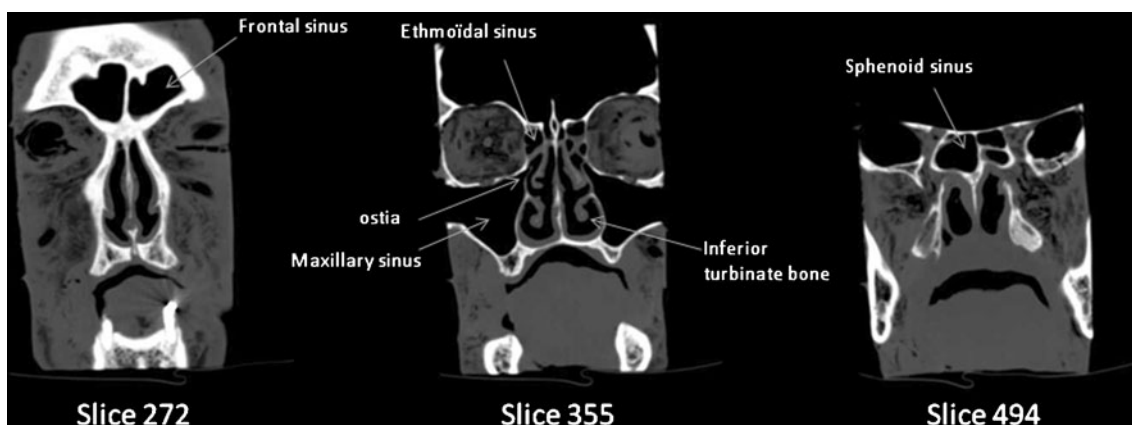


Fig. 1 CT scans of the plastinated head model (NC1).

Practice, all the volunteers gave their prior written informed consent. Exclusion criteria were the following: significant vascular or cardiac disease, history of allergy (e.g. allergic rhinitis) or asthma, and history of any ENT surgery (reconstructive or functional) or sinonasal pathology (e.g. nasal polyposis, chronic rhinosinusitis). Clinical examination was carried out by an ENT specialist. A right nasal septum deviation was detected in patient 3 and a right nasal bone spur in patient 5. These observations were considered as anatomical variants which may be encountered in a general non-selected population and these two volunteers were therefore included in the study. None of the subjects were taking any medication that might have had an effect on the upper airways during the study protocol.

Three gamma scintigraphy studies were performed for each volunteer: 81 m krypton gas ($^{81\text{m}}\text{Kr}$ gas) was administered to determine Regions Of Interest (ROIs) of the relevant anatomical volumes, and two aerosol deposition scintigraphies, one with the jet nebulizer and one with the mesh nebulizer. There was an interval of one month between the two aerosol scintigraphies.

Before the tests, volunteers were trained to inhale the aerosol through the nose and exhale through the mouth with the jet nebulizer, and to inhale and exhale only through the mouth with the mesh nebulizer. An absolute filter (BB50TE, Pall medical, Saint Germain-en-Laye, France) was connected to a mouthpiece, and an additional absolute filter was connected to the jet nebulizer to avoid ambient contamination. After nebulisation and during nasal image acquisition, volunteers inhaled and exhaled exclusively through the mouth as well as possible to avoid modification of activity distribution.

In Vivo Study

Two anatomical models of normal human nasal cavities were used: a plastinated head model (hereafter called NC1 for nasal cast 1), previously described and characterized by Durand et al. (18), and a 3D geometric replica of the plastinated head

model (hereafter called NC2 for nasal cast 2). The NC2 was designed from computed tomography images (CT scan) of the NC1 (Fig. 1) and made with Acrylonitrile Butadiene Styrene (ABS) using 3D imaging analysis and 3D printing technique (rapid prototyping by Fused Deposition Modelling (FDM)) (23). Solidworks 2012 software (Dassault Systems, Velizy-Villacoublay, France) was used for 3D reconstruction and Dimension 768 for printing (Dimension, Eden Prairie, USA; layer thickness: 0.245 mm (0.010 in.)). As in the *in vivo* study, three scintigraphic studies were performed with each *in vitro* model: $^{81\text{m}}\text{Kr}$ gas was administered to determine ROIs corresponding to the anatomical volumes, and two aerosol deposition scintigraphies, one with the jet nebulizer and one with the mesh nebulizer.

NC1 and NC2 were connected to a respiratory pump (Havard apparatus, Les Ulis, France; Tidal volume = 500 mL, I/E: 40/60, 15 breaths/min) *via* the rhinopharynx (Fig. 2). A specific one-way valve (resistance = 0.13 ± 0.07 cm $\text{H}_2\text{O}/\text{min}/\text{L}$, mean \pm SD measured for flow rates of 1 to 15 L/min) was connected to a T-piece equipped with an absolute filter, a tube (15 cm), and a second absolute filter, simulating respectively the soft palate and the mouth, the trachea and the lungs. The entirety was placed between the model and the pump.

In vitro experiments were designed to reproduce the *in vivo* aerosol administration conditions with both nebulizers (Fig. 2): nasal inhalation and mouth expiration with the jet nebulizer ($n=6$ for each nasal cast model), and mouth breathing only with the mesh nebulizer ($n=6$ for each nasal cast model).

Image Acquisition

All scintigraphic images (*in vivo* and *in vitro*) were recorded with a planar gamma camera (resolution 128×128) using a single detector equipped with a low-energy, high-resolution collimator. *In vivo* images were acquired with a Starport 400 AC/T camera (GE, Denmark - 390 mm collimator) calibrated monthly for uniformity (UFOV 370 mm and CFOV

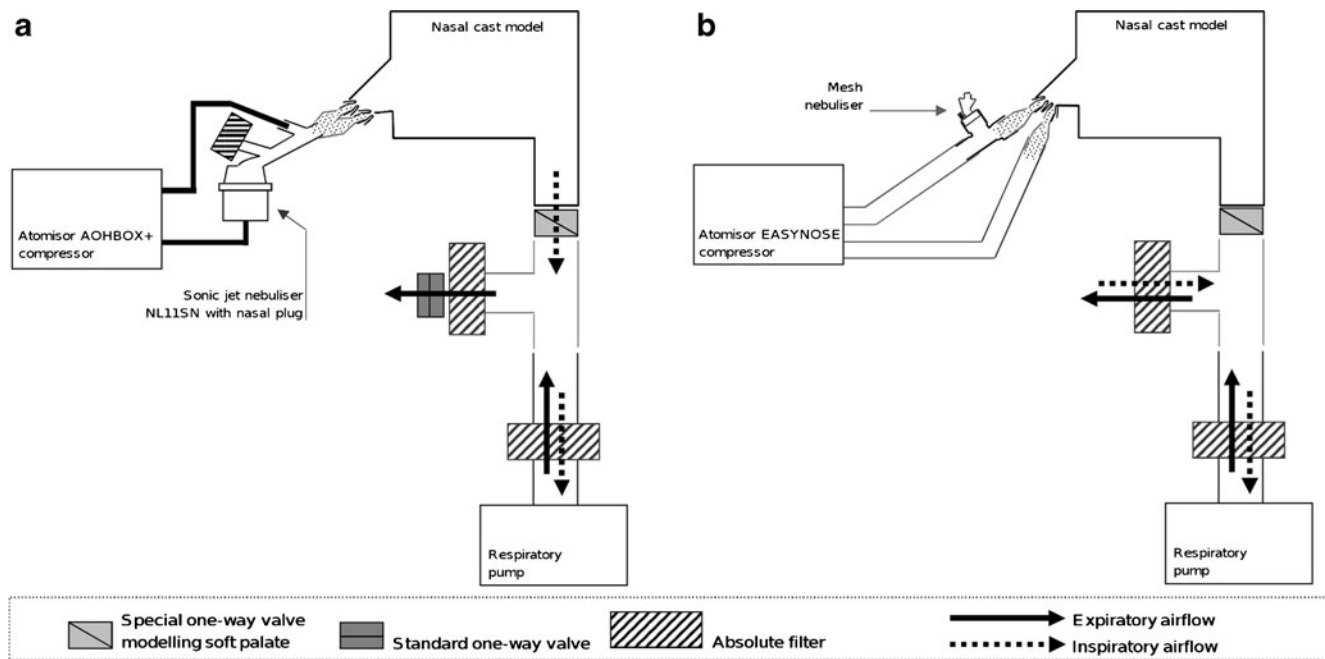


Fig. 2 *In vitro* experimental set-up.

278 mm). *In vitro* images were acquired with an E-cam camera (Siemens, Germany - 397 mm×500 mm collimator), also tested monthly for uniformity (UFOV 357 mm×475 mm, CFOV 268 mm×356 mm).

^{81m}Kr scintigraphies were performed before the aerosol deposition studies to define three ROIs: nasal, upper nasal cavity and maxillary sinus regions. Krypton ^{81m}Kr gas (⁸¹Rb-^{81m}Kr generator, Covidien, Petten, The Netherlands) was administered continuously through the nostrils of the volunteers, the NC1 and NC2 to outline nasal cavity volumes (Fig. 3). Three images of the volunteer’s head, the NC1 and the NC2 were acquired during 2 min of ^{81m}Kr gas inhalation: a lateral view of the nasal cavities to determine nasal and upper nasal cavity regions (Fig. 3), a coronal section of the nasal cavities, and a coronal section of the nasal cavities with an addition of 100Hz sound (AOLH box compressor) during gas administration to optimize definition of the maxillary sinus region (Fig. 4).

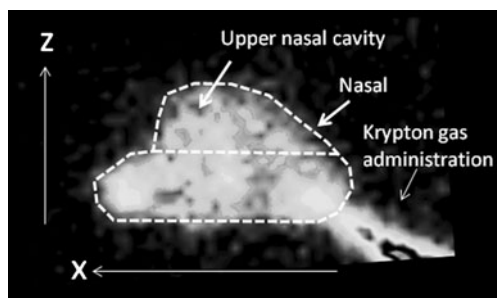


Fig. 3 Scintigraphy image of nasal krypton gas in volunteer and upper nasal cavity determination (lateral view).

Before aerosol inhalation, a nebulizer charge image was acquired over a 1-min period. After aerosol inhalation, the following images of volunteers and *in vitro* models were acquired over a 2-min period: a lateral view showing aerosol deposition in the nasal cavities and a coronal view showing deposition maxillary sinuses.

Image Processing

The ROIs were defined from the images obtained from ^{81m}Kr gas administration using Siemens software for the nose, and ImageJ software (ImageJ 1.43U, National Institutes of Health, USA) for the upper nasal cavity and maxillary sinuses. The upper nasal cavity region was defined as the upper half of the nasal region (lateral image) (Fig. 3). It contains the ethmoidal space, upper turbinates, the olfactory region and sphenoid regions. The maxillary sinuses were defined as the regions seen from the coronal view (Fig. 4). These ROIs were then applied to aerosol images to determine the radioactivity deposited in each region (nasal, upper nasal cavity and maxillary sinuses). For both *in vivo* and *in vitro* studies, the activity thus measured in the three ROIs was expressed in terms of the activity loaded into the nebulizer. All calculations took into account the background radiation and physical decay of radioactivity.

The gamma camera images were analyzed using ImageJ software. The distribution of the aerosol deposited in the nasal cavities was analyzed along three axes: the x-axis from the nostrils to the cavum (Fig. 3), the z-axis from the floor to the upper nasal cavities (Fig. 3), and the y-axis from the septum to the extremity of the maxillary sinuses (Fig. 4). *In vitro* and *in vivo*

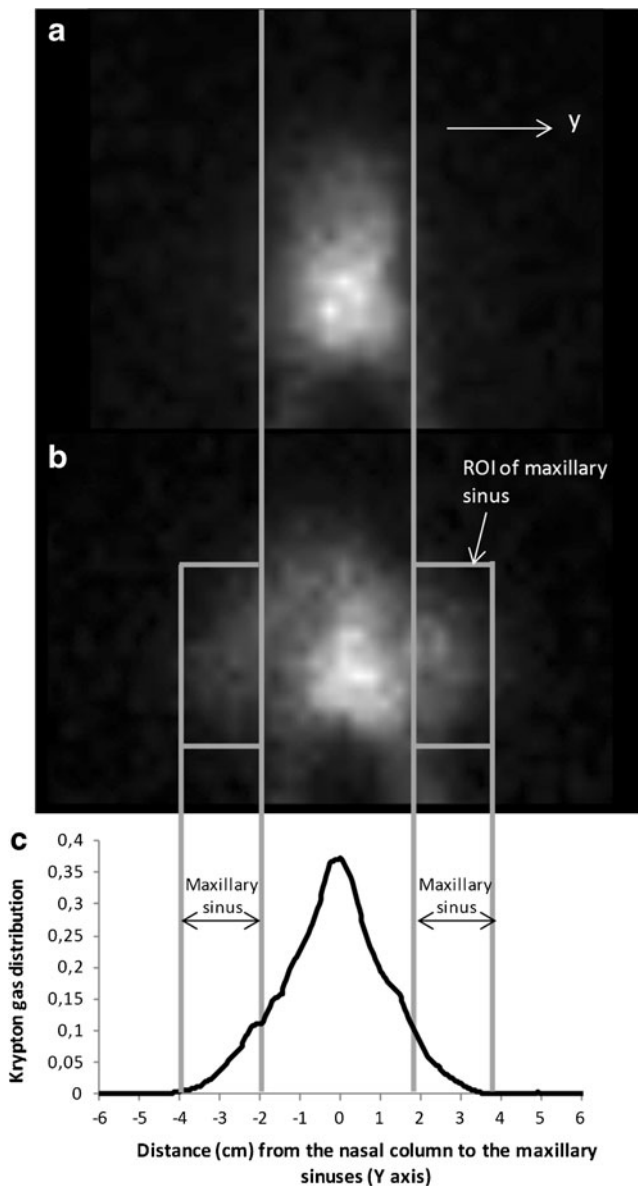


Fig. 4 (a) Scintigraphy image of nasal krypton gas in volunteer without sound (coronal view); (b) Scintigraphy image of nasal krypton gas in volunteer with 100Hz sound (coronal view); Krypton gas distribution in the nasal cavity of the volunteer and maxillary sinuses determination.

distributions were normalized taking into account the pixel size and counted radioactivity.

Statistical Analyses

Statistical analyses were performed using StatXact® software (StatXact-3 3.0.2, Cytel Software Corporation, France). Non-parametric stratified Normal Score tests were used to compare the *in vitro* and the *in vivo* aerosol deposition data for the three anatomical regions (nasal, upper nasal cavity and maxillary sinuses).

Standard Deviations (SD) of aerosol distribution along the three axes were calculated for the seven volunteers in the *in vivo* study, and the mean distribution was calculated for the six trials with the models in the *in vitro* study.

RESULTS

Regions of Interest

The nasal cavities of all volunteers, NC1 and NC2 were adequately imaged by krypton gas administration (Figs. 3 and 4). The addition of 100Hz sound during gas administration highlighted gas activity inside the maxillary sinuses of the volunteers (Fig. 4) and the nasal casts, demonstrating opening of the sinus ostia and sinus ventilation (). ImageJ analysis of ^{81m}Kr images provided an outline of nasal, upper nasal cavity and maxillary sinus regions in the volunteers and nasal casts.

Images of Aerosol Deposition

Figure 5 shows images of aerosol deposition in the nasal cavities of a volunteer (volunteer 6) and in NC1 and NC2 (profile view). Radioactive contamination of the lips occurred during inhalation with the mesh nebulizer and was observed in the volunteer's image (Fig. 5, *in vivo*-mesh). This contamination was not taken into account in the quantification of deposition in the nasal region. During *in vitro* experiments, radioactive drops running from the nose of the models were collected on absorbent paper to avoid model contamination and were also not taken into account in the quantification of deposition in the nasal region.

Nasal deposition was quantitatively similar in volunteers and in *in vitro* models. Aerosol administered by mesh nebulizer (upper images) was deposited from the nostrils (on the left) to the cavum (on the right), while jet nebulizer administration (lower images) resulted in a predominant deposition in the nasal valve.

Aerosol Deposition in Nasal Cavities

In vivo nasal aerosol deposition was $12.5 \pm 2.7\%$ with the mesh nebulizer and $3.7 \pm 1.1\%$ with the jet nebulizer. *In vitro* nasal aerosol deposition in NC1 was roughly similar to *in vivo* data: $10.8 \pm 1.5\%$ with the mesh nebulizer, and $3.2 \pm 0.3\%$ with the jet nebulizer ($p > 0.6$, Table I).

Within the nasal region, deposition in the upper nasal cavity and maxillary sinuses was similar in volunteers and NC1, for both types of nebulizer ($p > 0.1$, Table I) (upper nasal cavity: $1.6 \pm 0.7\%$ *in vivo* vs. $2.3 \pm 0.2\%$ in NC1 with the mesh nebulizer, $0.4 \pm 0.4\%$ *in vivo* vs. $0.5 \pm 0.1\%$ in NC1 with the jet nebulizer; maxillary sinuses: $0.9 \pm 0.5\%$ *in vivo* vs. $0.9 \pm 0.4\%$ in

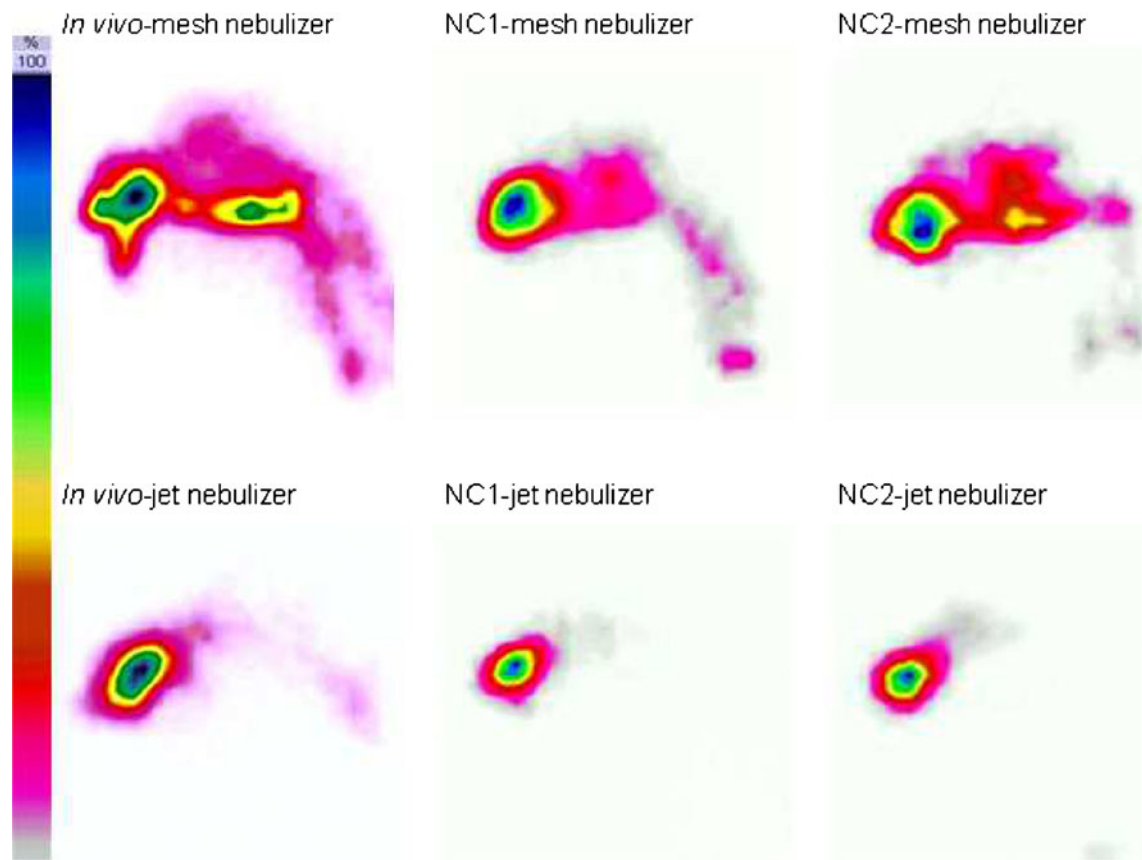


Fig. 5 Scintigraphy images of nasal aerosol deposition (right profiles) in volunteers (volunteer 6) and in two *in vitro* models (NC1 and NC2). Images were recorded after nasal inhalation of Tc^{99m} -DTPA aerosol with a mesh nebulizer (top images) and a jet nebulizer (bottom images).

NC1 with the mesh nebulizer, $0.2 \pm 0.1\%$ *in vivo* vs. $0.1 \pm 0.1\%$ in NC1 with the jet nebulizer).

Nasal deposition was significantly lower in NC2 ($7.2 \pm 1.0\%$ with the mesh nebulizer and $3.2 \pm 0.4\%$ with the jet nebulizer,

$p < 0.05$) than in volunteers, especially with the mesh nebulizer. However, deposition in the upper nasal cavity and maxillary sinuses of NC2 was similar to that of volunteers ($1.3 \pm 0.3\%$ (mesh nebulizer) and $0.3 \pm 0.1\%$ (jet nebulizer) in the upper nasal cavity; $0.7 \pm 0.2\%$, (mesh nebulizer) and $0.2 \pm 0.1\%$ (jet nebulizer) in maxillary sinuses; ($p > 0.7$) (Table I).

NC1 and NC2 differed significantly in aerosol deposition in the nasal and upper nasal cavity regions ($p < 0.05$).

Table I Aerosol Deposited (mean \pm SD) in Nasal Cavities (Nasal), Upper Nasal Cavity and Maxillary Sinus (MS) Regions of Healthy Volunteers (*In vivo*) and in Two Nasal Cast Models: NC1 and NC2, Expressed as a Percentage of the Nebulizer Charge

	<i>In vivo</i>	NC1	NC2
Mesh nebulizer			
Nasal	12.5 ± 2.7	$10.8 \pm 1.5^*$	$7.2 \pm 1.0^{**}$
Upper nasal cavity	1.6 ± 0.7	$2.3 \pm 0.2^*$	$1.3 \pm 0.3^*$
Maxillary sinuses	0.9 ± 0.5	$0.9 \pm 0.4^*$	$0.7 \pm 0.2^*$
Jet nebulizer			
Nasal	3.7 ± 1.1	$3.2 \pm 0.3^*$	$3.2 \pm 0.4^*$
Upper nasal cavity	0.4 ± 0.4	$0.5 \pm 0.1^*$	$0.3 \pm 0.1^*$
Maxillary sinuses	0.2 ± 0.1	$0.1 \pm 0.1^*$	$0.2 \pm 0.1^*$

*: no significant difference between NC1 and *In vivo* or no significant difference between NC2 and *In vivo* ($p > 0.1$), ** significant differences between NC1 and *In vivo* or between NC2 and *In vivo* ($p < 0.05$)

Aerosol Distribution in Nasal Cavities

Figure 6 shows the distribution of aerosol deposited between the nostrils and the rhinopharynx (x-axis), between the floor and the top of the nasal cavities (z-axis), and between the nasal column and the maxillary sinuses (y-axis).

All mean distributions of NC1 came within the SD of *in vivo* distribution, indicating similar distribution in volunteers and NC1. This close similarity was observed for both nebulizers, apart from a wider peak along the z-axis with the mesh nebulizer.

On the whole, mean distribution for NC2 came within the SD of *in vivo* distribution for both nebulizers. However, slight

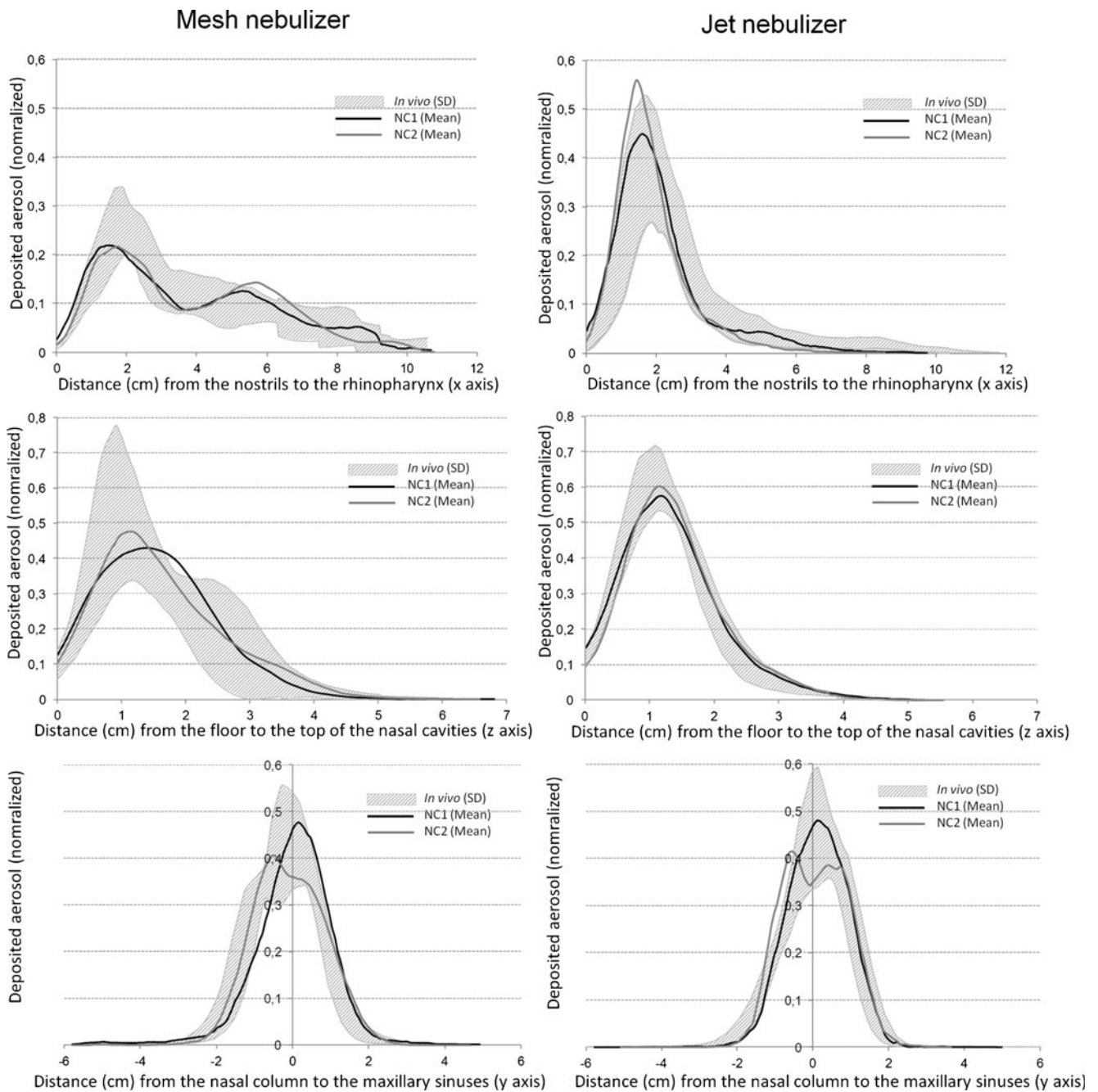


Fig. 6 Aerosol distributions (normalized) within the nasal cavities of volunteers (*in vivo*), the NC1 and the NC2, along three axes: x, y and z. *In vivo* results are represented by standard deviation (SD), and *in vitro* results by the mean.

differences were observed between the *in vivo* and NC2 profiles. The peak value of jet nebulizer distribution along the x-axis (from the nostrils to the rhinopharynx) was higher than the SD of *in vivo* distribution (Fig. 6). The peak of NC2 distribution along the y-axis was flatter than that of *in vivo* distribution.

As observed *in vivo*, the type of nebulizer affected distribution in both nasal casts (Fig. 6). Along the x-axis, the maximum value (2 cm from the nostrils, equivalent to the position of the

nasal valve) was higher with the jet nebulizer than with the mesh nebulizer. Deposition then decreased rapidly with the jet nebulizer and more slowly with the mesh nebulizer.

Along the z-axis, the SD of aerosol distribution in volunteers was similar with the two nebulizers, with a more proximal peak position with the jet nebulizer than with the mesh nebulizer. A second peak 2.5 cm from the nasal cavity floor was also observed, with a larger SD range with the mesh than with the jet nebulizer.

Along the y-axis, jet and mesh nebulizer distributions were similar, with a high deposition of aerosol along the nasal column (peak at 0 cm), decreasing on both sides of the nasal cavity up to the maxillary sinuses.

DISCUSSION

Our study demonstrates that the plastinated head model (NC1), but not the 3D geometric replica (NC2), enabled adequate prediction of aerosol deposition in nasal cavities, compared to scintigraphic measurements in human volunteers. Our results also demonstrate that the two nasal casts, despite having the same anatomical base, differ regarding intranasal aerosol deposition (Table I).

These differences could be explained by the fact that different methods were used to design these two models. The NC1 is an anatomical model, made from a cadaver head from which liquids and lipids have been extracted and replaced by silicone polymers. Bone, cartilage and mucosal tissue are preserved. Clinical examinations indicate that the anatomy and geometry of the nasal airways of the plastinated model are very similar to human anatomy (18). The procedure used to create NC2, the replica of NC1, requires 3D reconstruction and printing, and a chemical treatment to dissolve soluble support material. Consequently, its anatomy can differ from that of the original plastinated cast. Comparing the CT scans of the two nasal casts revealed generally similar anatomical structures (data not shown), but no quantitative comparison was performed. However, the analysis of krypton gas images revealed slight differences: the x-axis of NC2 was 6.5% shorter than that of NC1 (9.07 vs. 9.70 cm) and the z-axis 15.5% higher (4.97 vs. 4.30 cm). Meakin (23) measured differences of 10% (up to 36%) on several dimensions of an anatomical part and its ABS replica, indicating that FDM models are unsuitable for implant fitting. The z-axis measurement revealed a higher passage between the floor and the top of the nasal fossa, suggesting a larger ethmoid in NC2 than in NC1 (the upper nasal cavity ROI was defined as the upper half of the nasal cavity, thus the upper half of the z-axis). This can explain the fact that less aerosol was deposited in the upper nasal cavity region of NC2 than NC1 (1.3% vs. 2.3% of mesh nebulizer charge) and in the nose (7.2% vs. 10.8% of mesh nebulizer charge for NC2 and NC1 respectively). A similar result was described by Kelly *et al.* (21) in their study comparing particle deposition in Guilmette's models in which the total particle deposition was lower in those with a larger ethmoid volume. Moreover, due to anatomical imperfections of the NC1 at the level of the nasal valve, this part of the nasal septum was reconstructed slightly wider in NC2 (only observed on CT scans). This could explain the flatter peak obtained for NC2 along the y-axis (Fig. 6). Thus, the 3D reconstruction process, the 3D printing technology (fused deposition), its precision,

and the post-printing chemical action can all be sources of error in replicating a given model by FDM, leading to differences in aerosol deposition in NC1 and NC2.

Differences in design of the two models regarding the smoothness of the internal surface could also have affected airflow and aerosol deposition. The surface of NC2 is rough due to the building process (ABS layers fused), whereas the surface of NC1 is smooth, even slightly hydrophobic due to the use of silicone polymers. Surface imperfections can generate flow disturbances and increase aerosol droplet impaction and retention (21). This phenomenon, combined with a high velocity of aerosol flow, could explain the higher peak of the jet nebulizer's aerosol deposition along the x-axis before the nasal valve, indicating a high impaction of aerosol in this part of the nose (Fig. 6). The nasal valve is known to be a restricted passage for aerosol penetration in the posterior part of the nose; variations in the geometry and surface roughness (24) of this passage thus contributed to differences in distribution of the same aerosol in NC2 and NC1. Maximum aerosol delivery time was 10 min and a total volume of 3 ml was loaded in the nebulizer. This may have resulted in significant overload at some locations, such as the nasal valve, dripping out part of the radioactive deposit, and in lip contamination as observed in the gamma camera image of some healthy volunteers. To avoid potential artefacts due to lip contamination, we applied the ROIs (determined by the krypton gas images) precisely to the aerosol image. In this way, the lip contamination was excluded from the ROIs and was thus not counted in the activity deposited in the nasal cast. Furthermore, to limit the modification of the location of the activity due to high deposited volume and dripping, the human volunteers had been trained to inhale exclusively through the mouth after aerosol administration to avoid modification of the activity location as the *in vitro* model. Thus, although there is a risk of an overload of deposited aerosol and consequently a modification of activity distribution in the nasal cavity, *in vivo* and *in vitro* models used the same protocol taking into account this potential modification of activity distribution.

Furthermore, the two models were designed using different materials, which could have influenced the radioactive count with the gamma imager. The material of NC1 is similar to human tissue whereas NC2 is made of plastic. The two materials showed a different pattern of radioactive attenuation: an attenuation image (profile) was obtained by setting the model between a radioactive phantom (74 MBq) and the camera collimator. The radioactive attenuation profile was more heterogeneous for NC1 (differences between anatomical areas) than for NC2. The percentage of radioactive attenuation, calculated as the mean of the whole model, was similar in the two models: 46% for NC1 and 47% for NC2. However, differences in the distribution of this attenuation along the

three nasal cavity axes could be considered as a source of error in the analysis of radioactive aerosol distribution and in the measurement of radioactivity in the different ROIs.

Mucociliary clearance was totally absent in our models. This could limit prediction of *in vivo* deposition. Indeed, the physiology of the nose affects intranasal drug deposition and clearance and thus its bioavailability. The anterior part of the nose is considered to be a non-ciliated area, in contrast to the more posterior part, beyond the nasal valve (25). Thus, drug clearance can differ depending on the initial deposition site. Without mucociliary clearance, the distribution recorded in our nasal models should reflect the initial aerosol deposition of the radioactive tracer, in contrast to distribution recorded in volunteers who had a mean nasal clearance of 6 to 10 mm/min (12). However, *in vivo* and *in vitro* distributions were still similar. Our study suggests that some kind of clearance or nasal mucus occurred in the nasal models after 10 min of liquid nebulisation. Möller *et al.* (26) investigated the nasal clearance of inhaled aerosol in human volunteers and obtained 50% of radioactive tracer clearance in more than 1 h using aerosol devices similar to those used in our study. Möller also found that this clearance occurred significantly later with a nebulizer than with a nasal spray, leading to a high deposition of the radioactive tracer in the nose and on the nasal cavity floor (50% of nasal clearance in less than 30 min). Both the human volunteers and the nasal cast models represent healthy human nose anatomies which are different from those found in nasal airway diseases, such as chronic rhinosinusitis (CRS) where the nasal mucosa is inflamed, with obstruction of the nasal airways and limited access to the sinus cavities. Recommended treatment for CRS is first nasal saline irrigation, intranasal corticosteroids, and oral antibiotics, and secondly sinus surgery, but 27% of patients with surgery show no symptomatic improvement (27).

A recent bacteriological study of ethmoid specimens taken from patients with nasal polyposis after ethmoidal surgery found that nearly all the microorganisms were susceptible to antibiotics (28). Directed nebulized antibiotic therapy may be a treatment option for patients with CRS refractory to conventional treatments (29). Atomisor sonique® nebulizer has demonstrated its ability to administrate aerosol and more particularly antibiotics into maxillary sinuses (30). Atomisor sonique® may therefore have clinical potential. However, differences in the anatomy of healthy individuals and patients with nasal airway disease could result in differences in aerosol deposition and affect the efficacy of therapy. Our method could be used in cases of nasal airway disease to optimize aerosol delivery devices for specific indications.

In conclusion, the present study demonstrates that the deposition of nebulized aerosols in human nasal cavities could be predicted using a nasal cast but not with its replica due to not optimal technical work.

The prediction of deposition differs according to the nasal model used and the accuracy of the prediction depends on the quality of the model.

ACKNOWLEDGMENTS AND DISCLOSURES

Sandrine LeGuellec, Stephane Gatier and Laurent Vecellio are employed by DTF.

Open Access This article is distributed under the terms of the Creative Commons Attribution License which permits any use, distribution, and reproduction in any medium, provided the original author(s) and the source are credited.

REFERENCES

1. Fokkens WJ, Lund VJ, Mullol J, Bachert C, Alobid I, *et al.* European position paper on rhinosinusitis and nasal polyps. *Rhinol Suppl.* 2012;3:1–298.
2. Costantino HR, Illum L, Brandt G, Johnson PH, Quay SC. Intranasal delivery: physicochemical and therapeutic aspects. *Int J Pharm.* 2007;7(337):1–24.
3. Laube BL. The expanding role of aerosols in systemic drug delivery, gene therapy, and vaccination. *Respir Care.* 2005;50:1161–76.
4. Costantino HR, Sileno AP, Johnson PH. Pharmacokinetic attributes of intranasal delivery: case studies and new opportunities. *Drug Deliv.* 2005;3:8–11.
5. Grassin-Delyle S, Buenestado A, Naline E, Faisy C, Blouquit-Laye S, *et al.* Intranasal drug delivery: an efficient and non-invasive route for systemic administration: focus on opioids. *Pharmacol Ther.* 2012;134:366–79.
6. Illum L. Is nose-to-brain transport of drugs in man a reality? *J Pharm Pharmacol.* 2004;56:3–17.
7. Illum L, Watts P, Fisher AN, Hinchcliffe M, Norbury H, *et al.* Intranasal delivery of morphine. *J Pharmacol Exp Ther.* 2002;301:391–400.
8. Banks WA, Doring MJ, Niehoff ML. Brain uptake of the glucagon-like peptide-1 antagonist exendin after intranasal administration. *J Pharmacol Exp Ther.* 2004;309:469–75.
9. Jogani VV, Shah PJ, Mishra P, Mishra AK, Misra AR. Nose-to-brain delivery of tacrine. *J Pharm Pharmacol.* 2007;59:199–205.
10. Jogani VV, Shah PJ, Mishra P, Mishra AK, Misra AR. Intranasal mucoadhesivemicroemulsion of tacrine to improve brain targeting. *Alzheimer Dis Assoc Disord.* 2008;22:116–24.
11. Laube B. Devices for aerosol delivery to treat sinusitis. *J Aerosol Med.* 2007;20:5–18.
12. Baroody FM. Nasal and paranasal sinus anatomy and physiology. *Clin Allergy Immunol.* 2007;19:1–21.
13. Jogani V, Jinturkar K, Vyas T, Misra A. Recent patents review on intranasal administration for CNS drug delivery. *Recent Pat Drug Deliv Formul.* 2008;2:25–40.
14. Rapoport AM. The therapeutic future in headache. *Neurol Sci.* 2012;33:S119–25.
15. FDA Guidance for Industry. Nasal Spray and Inhalation Solution, Suspension, and Spray Drug Products - Chemistry, Manufacturing, and Controls Documentation. U.S. Department of Health and Human Services Food and Drug Administration Center for Drug Evaluation and Research. 2002.
16. Vecellio L, De Gerssem R, Le Guellec S, Reychler G, Pitance L, *et al.* Deposition of aerosols delivered by nasal route with jet and mesh nebulizers. *Int J Pharm.* 2011;407:87–94.

17. Valentine R, Athanasiadis T, Thwin M, Singhal D, Weitzel EK, Wormald PJ. A prospective controlled trial of pulsed nasal nebulizer in maximally dissected cadavers. *Am J Rhinol*. 2008;22:390–4.
18. Durand M, Pourchez J, Louis B, Pouget JF, Isabey D, *et al*. Platinated nasal model: a new concept of anatomically realistic cast. *Rhinology*. 2011;49:30–6.
19. Möller W, Schuschnig U, Meyer G, Mentzel H, Keller M. Ventilation and drug delivery to the paranasal sinuses: studies in a nasal cast using pulsating airflow. *Rhinology*. 2008;46:213–20.
20. Kundoor V, Dalby RN. Assessment of nasal spray deposition pattern in a silicone human nose model using a color-based method. *Pharm Res*. 2010;27:30–6.
21. Kelly JT, Asgharian B, Kimbell JS, Wong BA. Particle deposition in human nasal airway replicas manufactured by different methods. Part I: inertial regime particles. *Aerosol Sc Technol*. 2004;38:1063–71.
22. Janssens HM, de Jongste JC, Fokkens WJ, Robben SG, Wouters K, Tiddens HA. The Sophia Anatomical Infant Nose-Throat (Saint) model: a valuable tool to study aerosol deposition in infants. *J Aerosol Med*. 2001;14:433–41.
23. Meakin JR, Shepherd DE, Hukins DW. Short communication: fused deposition from CT scans. *Br J Radiol*. 2004;77:504–7.
24. Schroeter JD, Garcia GJ, Kimbell JS. Effects of surface smoothness on inertial particle deposition in human nasal models. *J Aerosol Sci*. 2011;42:52–63.
25. Vidgren MT, Kublik H. Nasal delivery systems and their effect on deposition and absorption. *Adv Drug Deliv Rev*. 1998;29:157–77.
26. Möller W, Saba GK, Haussinger K, Becker S, Keller M, Schuschnig U. Nasally inhaled pulsating aerosols: lung, sinus and nose deposition. *Rhinology*. 2011;49:286–91.
27. Al Badaai Y, Samaha M. Outcome of endoscopic sinus surgery for chronic rhinosinusitis patients: a Canadian experience. *J Laryngol Otol*. 2010;124:1095–9.
28. Day N, Mainardi JL, Malinvaud D, Bonfils P. Bacteriological study of ethmoid specimens from patients with nasal polyposis after ethmoidal surgery. *Ann Otolaryngol Chir Cervicofac*. 2009;126:196–202.
29. Woodhouse BM, Cleveland KW. Nebulized antibiotics for the treatment of refractory bacterial chronic rhinosinusitis. *Ann Pharmacother*. 2011;45:798–802.
30. Durand M, Pourchez J, Aubert G, Le Guellec S, Navarro L, Forest V, *et al*. Impact of acoustic airflow nebulization on intrasinus drug deposition of a human platinated nasal cast: new insights into the mechanisms involved. *Int J Pharm*. 2011;12:63–71.